Stem Cell Reports
Article

OPEN ACCESS

Proteinase 3 Limits the Number of Hematopoietic Stem and Progenitor Cells in Murine Bone Marrow

Kutay Karatepe,[1,2,6] Haiyan Zhu,[3,5,6] Xiaoyu Zhang,[1,2] Rongxia Guo,[3] Hiroto Kambara,[1,2] Fabien Loison,[1,2] Peng Liu,[3] Hongbo Yu,[4] Qian Ren,[3] Xiao Luo,[1,2] John Manis,[1,2] Tao Cheng,[3] Fengxia Ma,[3] Yuanfu Xu,[3,*] and Hongbo R. Luo[1,2,*]

[1]Department of Lab Medicine, The Stem Cell Program, Boston Children's Hospital, Boston, MA 02115, USA
[2]Department of Pathology, Harvard Medical School, Dana-Farber/Harvard Cancer Center, Boston, MA 02115, USA
[3]The State Key Laboratory of Experimental Hematology, Institute of Hematology and Blood Diseases Hospital, Chinese Academy of Medical Sciences and Peking Union Medical College, 288 Nanjing Road, Tianjin 300020, China
[4]VA Boston Healthcare System, Department of Pathology and Laboratory Medicine, 1400 VFW Parkway, West Roxbury, MA 02132, USA
[5]Present address: Department of Clinical Lab, Weihai Municipal Hospital, Affiliated to Dalian Medical University, Weihai, Shandong 264200, China
[6]Co-first author
*Correspondence: xuyf@ihcams.ac.cn (Y.X.), hongbo.luo@childrens.harvard.edu (H.R.L.)
https://doi.org/10.1016/j.stemcr.2018.10.004

SUMMARY

Hematopoietic stem and progenitor cells (HSPCs) undergo self-renewal and differentiation to guarantee a constant supply of short-lived blood cells. Both intrinsic and extrinsic factors determine HSPC fate, but the underlying mechanisms remain elusive. Here, we report that Proteinase 3 (PR3), a serine protease mainly confined to granulocytes, is also expressed in HSPCs. PR3 deficiency intrinsically suppressed cleavage and activation of caspase-3, leading to expansion of the bone marrow (BM) HSPC population due to decreased apoptosis. PR3-deficient HSPCs outcompete the long-term reconstitution potential of wild-type counterparts. Collectively, our results establish PR3 as a physiological regulator of HSPC numbers. PR3 inhibition is a potential therapeutic target to accelerate and increase the efficiency of BM reconstitution during transplantation.

INTRODUCTION

The hematopoietic system is responsible for replenishing short-lived blood cells while regulating the differentiation, self-renewal, and apoptosis of hematopoietic stem cells (HSCs) in the bone marrow (BM). The most primitive HSCs give rise to multilineage hematopoietic progenitor cells (HPCs) capable of producing unilineage progenitors that later differentiate into mature blood cells (Orkin and Zon, 2008). Various aspects of this well-defined hierarchy, such as the relative contribution of HSCs to the peripheral cell pool and the presence of HPCs in adult BM, have recently been challenged (Notta et al., 2016; Sun et al., 2014). Similarly, the nature and regulation of hematopoietic stem and progenitor cell (HSPC) lifespan and apoptosis are not well defined.

HSCs are mostly quiescent with a finite lifespan (Cheshier et al., 1999; Sieburg et al., 2011). Cell cycling and apoptosis in HSCs are dynamically regulated according to context (Takizawa et al., 2011). Deletion of anti-apoptotic *Mcl-1* leads to HSC death (Opferman et al., 2005), while overexpression of anti-apoptotic *Bcl-2* (Domen et al., 2000) or deficiency of pro-apoptotic *Caspase 3* (Janzen et al., 2008) enhances HSC survival. Inhibition of caspase activity facilitates engraftment of donor HSCs and accelerates donor hematopoiesis in a mouse BM transplantation model (Imai et al., 2010). Caspase inhibition in human $CD34^+$ cells results in higher engraftment in NOD/SCID mice, enhanced clonogenicity, and long-term culture-initiating potential *in vitro* (V et al., 2010). Also, microRNA miR-125a reduces apoptosis of HSPCs and expands the HSPC pool (Guo et al., 2010). However, the mechanisms that regulate apoptosis in HSPCs are not as well understood as those regulating cell cycling.

Proteinase 3 (PR3; encoded by *Prtn3*) was originally termed myeloblastin due to its ability to induce proliferation and inhibit differentiation of HL-60 cells, a promyelocytic leukemia cell line (Bories et al., 1989). *Prtn3* is mainly expressed in granulocytes and granulocyte progenitors. PR3 is a neutrophil serine protease family member whose roles in bacterial killing and post-translational modification of cytokines have been extensively studied in neutrophils (Campanelli et al., 1990; Coeshott et al., 1999). We recently reported that PR3 regulates neutrophil spontaneous death by cleaving and activating procaspase-3 (Loison et al., 2014). Surprisingly, here we report that PR3 is also highly expressed in the HSPC compartment and regulates the survival as well as engraftment of HSPCs. PR3 deficiency reduced programmed cell death of HSPCs and expanded their population in the BM. The long-term reconstitution potential of PR3-deficient HSPCs was increased. Collectively, these findings suggest that PR3 limits the number of HSPCs in murine BM.

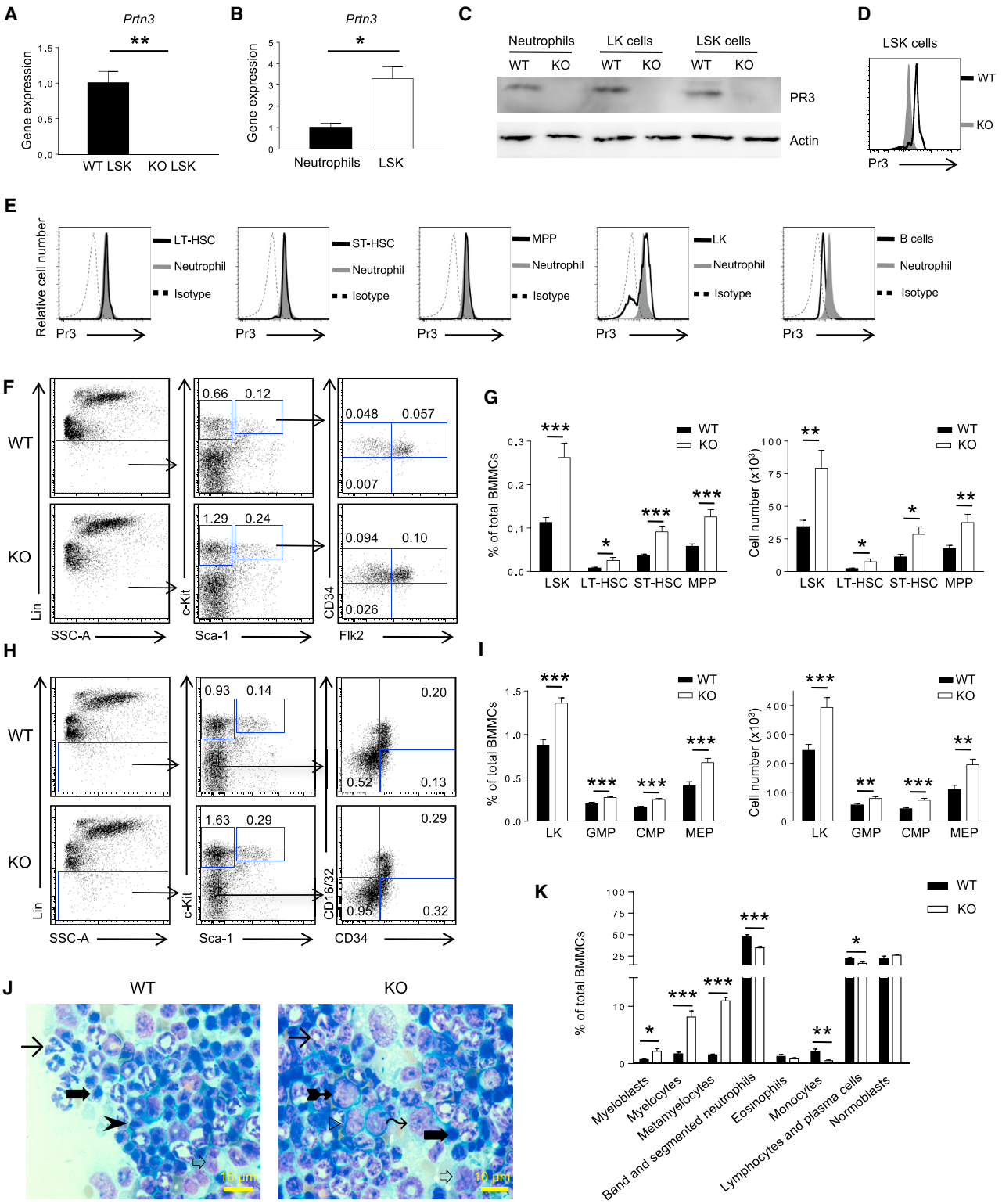

Figure 1. *Prtn3* Is Expressed in Hematopoietic Stem/Progenitor Cells and Regulates the Number of Stem and Progenitor Cell Subsets

(A) *Prtn3* mRNA expression in sorted BM stem cell-containing populations (LSK cells) in WT and *Prtn3*$^{-/-}$ mice as determined by quantitative RT-PCR (n = 3 per group).

(legend continued on next page)

RESULTS

Prtn3 Is Expressed in Hematopoietic Stem and Progenitor Cells

To address whether *Prtn3* expression in BM is restricted to neutrophils and myeloid progenitors, we assayed highly purified LSK cells ($Lin^-c\text{-}Kit^+Sca1^+$) and neutrophils ($Gr1^+CD11b^+$) from *Prtn3*-deficient ($Prtn3^{-/-}$) and control wild-type (WT) mice. High *Prtn3* transcript levels were detected in WT but not $Prtn3^{-/-}$ LSK cells (Figures 1A and S1A). Quantification of mRNA revealed 2-fold higher *Prtn3* mRNA expression in LSK cells compared with neutrophils (Figure 1B). Examination of two publicly available transcriptome databases of hematopoietic cells revealed the highest *Prtn3* expression in primitive HSCs (Figures S1B and S1C) (Chambers et al., 2007; Hyatt et al., 2006). *Prtn3* was also detected at the protein level in LSK cells and lineage negative, c-Kit positive, and Sca-1 negative (LK) cells (which include myeloid progenitor cells) as assayed by western blotting and flow cytometry (Figures 1C–1E and S1D). Comparison of PR3 expression among different LSK subsets by conventional flow cytometry revealed that $CD34^-Flk2^-$ long-term (LT) HSCs, $CD34^+Flk2^-$ short-term (ST) HSCs, and $CD34^+Flk2^+$ multipotent progenitors (MPPs) expressed PR3 at levels comparable with neutrophils (Figure 1E).

Prtn3 Deficiency Leads to an Increase in the Number of Stem, Progenitor, and Immature Myeloid Cells in the Murine BM

Due to high *Prtn3* expression in HSPCs, we explored whether PR3 modulates hematopoiesis *in vivo*. $Prtn3^{-/-}$ spleens weighed less than those from WT mice despite no difference in body weight, BM cellularity, and total blood cell count (Figures S1E–S1G). The peripheral blood contained a slightly higher percentage of myeloid cells and a slightly lower percentage of lymphoid cells in $Prtn3^{-/-}$ mice compared with WT mice, while other parameters were unchanged (Figure S1H). We next examined the overall frequency and numbers of HSPCs in the BM of WT and $Prtn3^{-/-}$ mice. The frequency and absolute number of LSK cells in $Prtn3^{-/-}$ mice was twice that of controls. Expansion of the LSK compartment was not restricted to a specific LSK subset: both the proportions and numbers of LT-HSCs, ST-HSCs, and MPPs were higher in $Prtn3^{-/-}$ BM (Figures 1F and 1G). The $CD150^+CD48^-$ LSK cell compartment was also enhanced in $Prtn3^{-/-}$ mice (Figures S1I and S1J). The proportion and number of LK cells, the HPCs that can give rise to myeloid or erythroid lineages, was 50% higher in $Prtn3^{-/-}$ BM. When the LK population was subfractionated into $CD34^-CD16/32^-$ megakaryocyte/erythroid progenitors (MEPs), $CD34^+CD16/32^-$ common myeloid progenitors, and $CD34^+CD16/32^+$ granulocyte/monocyte progenitors, the frequency and number of all three subpopulations was increased in $Prtn3^{-/-}$ BM (Figures 1H and 1I).

Given the increased number of stem and progenitor cells in $Prtn3^{-/-}$ mice, we next determined the frequency of cells at different stages of myeloid and lymphoid development. Histological analysis of BM smears from WT and $Prtn3^{-/-}$ mice revealed an increased frequency of immature myeloid cells such as myeloblasts, myelocytes, and metamyelocytes in $Prtn3^{-/-}$ BM and decreased frequencies of band and segmented neutrophils and lymphocytes (Figures 1J and 1K). Collectively, these results indicate that *Prtn3*

(B) Comparison of *Prtn3* mRNA expression in sorted LSK cells and neutrophils from WT mice. *GAPDH* was used as a housekeeping control (n = 3 per group).
(C) PR3 protein expression in sorted BM stem (LSK) and progenitor (LK) cell-containing populations and neutrophils as determined by western blotting. Pan-actin was used as a loading control. Results are representative of three independent experiments.
(D) Intracellular PR3 staining in LSK cells from WT and $Prtn3^{-/-}$ BM by conventional flow cytometry. Results are representative of five independent experiments.
(E) Intracellular PR3 staining in different cell populations as determined by conventional flow cytometry. Results are representative of five independent experiments.
(F) Representative flow cytometry plots for LSK subsets in WT and $Prtn3^{-/-}$ mice. Numbers denote the frequency of each population among live singlets.
(G) Quantification of the frequency and number (per one femur and one tibia) of LSK subsets in WT and $Prtn3^{-/-}$ mice (n = 10 per group).
(H) Representative flow cytometry plots for LK subsets in WT and $Prtn3^{-/-}$ mice. Numbers denote the frequency of each population among live singlets.
(I) Quantification of the frequency and number of LK subsets in WT and $Prtn3^{-/-}$ mice (n = 16 per group).
(J) Representative images of histological analysis of BM smears from WT and *Prtn3*−/− mice. Arrowhead, lymphocyte; long arrow, neutrophil; thick arrow, normoblast; white arrow, monocyte; tailed arrow, myelocyte; right-pointing triangle, myeloblast; wavy arrow, metamyelocyte.
(K) Quantification of cells belonging to different lineages and maturation stages according to histological analysis of BM smears (n = 6 per group).
Scale bar, 10 μm. All values shown are means ± SEM. *p < 0.05, **p < 0.01, ***p < 0.001, by unpaired, 2-tailed Student's t test. See also Figure S1.

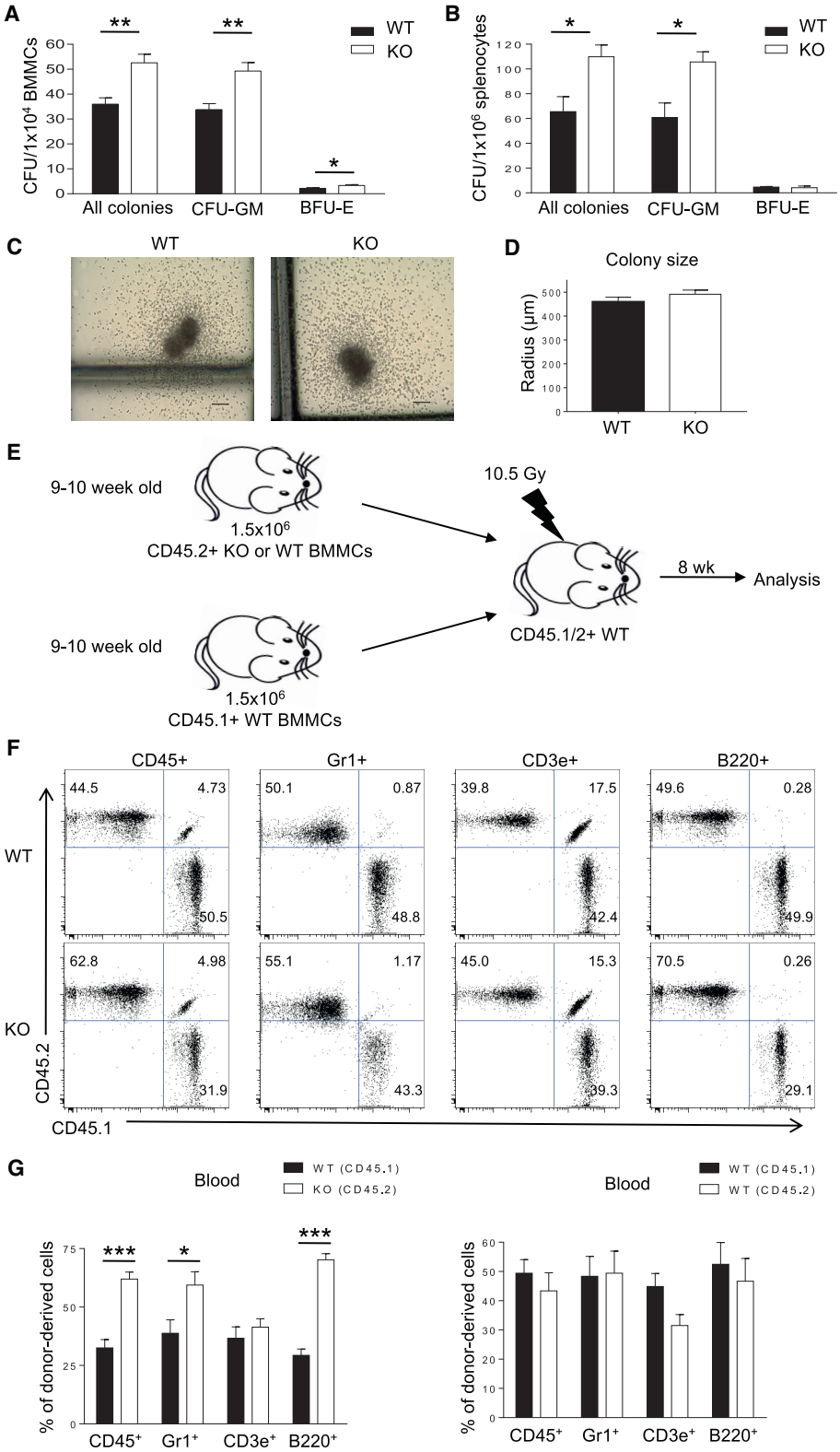

(legend on next page)

disruption expands HSPCs and enhances hematopoiesis, particularly myelopoiesis.

The Expanded HPC Compartment in *Prtn3*$^{-/-}$ Bone Marrow Is Functionally Active Both *In Vitro* and *In Vivo*

To test if the expanded HPC compartment in *Prtn3*$^{-/-}$ mice is functional *in vitro*, we performed colony-forming cell (CFC) assays. Myeloid and erythroid CFC assays with total BM cells confirmed an increase in the number of functional progenitors in *Prtn3*$^{-/-}$ mice *in vitro* (Figure 2A). Splenocytes from *Prtn3*$^{-/-}$ mice also gave rise to more colonies than those from WT mice (Figure 2B), suggesting that the enhanced HPC compartment in *Prtn3*$^{-/-}$ mice is not BM restricted. Of note, WT and *Prtn3*$^{-/-}$ total BM-derived colonies were of similar size (Figures 2C and 2D). To examine whether early progenitor cells in *Prtn3*$^{-/-}$ mice could outcompete WT cells *in vivo*, we transplanted total BM cells from WT and *Prtn3*$^{-/-}$ mice into lethally irradiated congenic recipients in a competitive BM transplantation setting (Figure 2E). At 8 weeks post transplant, peripheral blood cells were analyzed for donor contribution by lineage analysis. The *Prtn3*$^{-/-}$ donor gave rise to more total white blood, myeloid, and B cells, but not T cells, than the WT donor (Figures 2F and 2G). Taken together, these results confirm that *Prtn3* disruption expands functionally active HPCs.

Disruption of *Prtn3* Accelerates BM Recovery after Irradiation

Expansion of HPCs often improves BM recovery after damage, so we investigated whether *Prtn3* disruption improves BM recovery in irradiated mice. WT and *Prtn3*$^{-/-}$ mice were sublethally irradiated (4 Gy), and hematopoietic recovery was assessed by analyzing peripheral blood, BM, and spleen at various time points (Figure 3A). Starting at 7 days post irradiation, *Prtn3*$^{-/-}$ mice had higher numbers of total white blood cells in the peripheral blood (Figure 3B). Various lineages in the peripheral blood including neutrophils, monocytes, lymphocytes, and eosinophils exhibited faster recovery in *Prtn3*$^{-/-}$ mice (Figure 3C). Meanwhile, the recovery of red blood cells and hemoglobin was slightly delayed in *Prtn3*$^{-/-}$ mice (Figure S2A), a phenotype also manifested intriguingly in the aged murine hematopoietic system (Florian et al., 2012). It may suggest myeloid skewing in the myeloid/erythroid differentiation program, with a corresponding higher granulocyte/erythroid ratio. *Prtn3*$^{-/-}$ mice had higher body weight after irradiation (Figure S2B). While other factors such as reduced intestinal damage may also be responsible for higher body weight after total body irradiation, *Prtn3*$^{-/-}$ mice also had higher BM cellularity 7 days post irradiation (Figure 3D). BM analysis showed that neutrophil, T cell, B cell, and LK cell recovery was more rapid in the BM of *Prtn3*$^{-/-}$ mice (Figures 3E–3G). Similarly, splenocytes and the numbers of different cell lineages in the spleen showed a similar recovery pattern (Figures S2C–S2E). An interesting finding that was observed in this study was the extreme fluctuation between day 7 and day 18 with respect to myeloid and B cell recovery (Figures 3C and 3F). We suspect two different progenitor populations are responsible for producing the peripheral blood cells observed on these time points. Nevertheless, these results suggest that *Prtn3*$^{-/-}$ mice are more resistant to hematopoietic injury at all time points analyzed.

To assess if the quicker hematopoietic recovery in *Prtn3*$^{-/-}$ mice translated to survival, WT and *Prtn3*$^{-/-}$ mice were irradiated with a higher dose (7.8 Gy), and survival rates were monitored for 30 days. WT mice started dying around day 10 and had a survival rate of about 10% on day 20 post irradiation. In contrast, *Prtn3*$^{-/-}$ mice had a survival rate of 50% on day 20 post irradiation (Figure 3H). Collectively, CFC assays, competitive BM reconstitution, and sublethal irradiation experiments all show that the enhanced HPC compartment in *Prtn3*$^{-/-}$ BM is functional *in vitro* and *in vivo*.

Elevated Hematopoiesis Caused by *Prtn3* Disruption Is an Intrinsic Feature of HSCs

To further delineate whether the enhanced hematopoiesis in *Prtn3*$^{-/-}$ mice is an intrinsic feature of HSCs,

Figure 2. Expanded Hematopoietic Progenitor Cell Compartment in *Prtn3*$^{-/-}$ Bone Marrow Is Functionally Active.

(A) Quantification of *in vitro* progenitor cell activity as demonstrated by colony-forming cell assays using BM cells (n = 9 per group).

(B) Quantification of *in vitro* progenitor cell activity as demonstrated by colony-forming cell assays using splenocytes (n = 3 per group).

(C) Representative images of WT and *Prtn3*$^{-/-}$ colonies from colony-forming cell assays. Scale bar, 100 μm.

(D) Quantitative analysis of colony sizes from WT and *Prtn3*$^{-/-}$ colonies. The sizes of at least ten colonies were measured per sample (n = 6 per group).

(E) Scheme of the experimental setup for the competitive bone marrow transplantation.

(F) Representative FACS dot plots for myeloid cells, B cells, and T cells showing the reconstitution capacity of different donors in the recipient mice.

(G) Quantitative analysis of the distribution of cells in the recipient mice at 8 weeks post transplantation (n = 4 per group). Results are representative of two independent experiments.

All values shown are means ± SEM. *p < 0.05, **p < 0.01, ***p < 0.001, by unpaired, 2-tailed Student's t test.

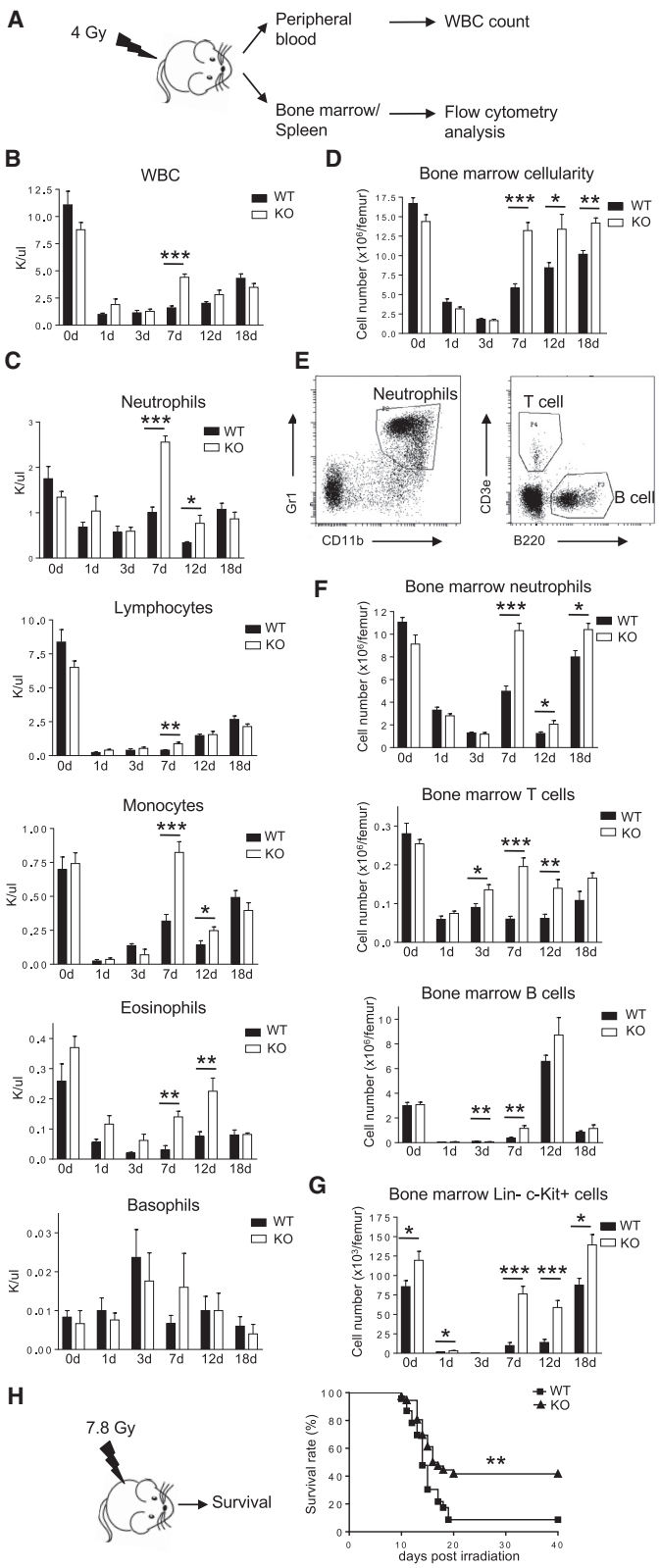

Figure 3. The Expanded Hematopoietic Progenitor Cell Population in *Prtn3*$^{-/-}$ Bone Marrow Provides Faster Recovery and Increased Survival after Hematopoietic Injury

(A) The experimental setup used to analyze hematopoietic recovery after challenge with sublethal irradiation (4 Gy).

(B) Total white blood cell counts in WT and *Prtn3*$^{-/-}$ mice before and after sublethal irradiation (n = 5–9 per group).

(C) Neutrophil, lymphocyte, monocyte, eosinophil, and basophil cell counts in WT and *Prtn3*$^{-/-}$ mice before and after sublethal irradiation (n = 5–9 per group).

(D) The number of BM mononuclear cells per one femur in WT and *Prtn3*$^{-/-}$ mice before and after sublethal irradiation (n = 5–9 per group).

(E) Representative FACS dot plots for identifying the frequencies of neutrophils, T cells, and B cells in the BM.

(F) Quantitative analysis of neutrophils, T cells, and B cells per one femur in WT and *Prtn3*$^{-/-}$ mice before and after sublethal irradiation (n = 5–9 per group).

(G) Quantitative analysis of LK cells per one femur in WT and *Prtn3*$^{-/-}$ mice before and after sublethal irradiation (n = 5–9 per group).

(H) Scheme of the experimental setup for survival analysis after challenge with 7.8 Gy irradiation and the survival curves of WT and *Prtn3*$^{-/-}$ mice receiving 7.8 Gy irradiation (n = 23 for WT and n = 36 for *Prtn3*$^{-/-}$).

All values shown are means ± SEM. *p < 0.05, **p < 0.01, ***p < 0.001, by unpaired, 2-tailed Student's t test (A–G) and log rank (Mantel-Cox) test for survival curve (H). See also Figure S2.

we competitively transplanted LSK cells from WT and *Prtn3*$^{-/-}$ mice with supporting cells into lethally irradiated WT congenic recipients (Figure 4A). BM and peripheral blood compartments were examined at 16 weeks post transplant to assess the long-term reconstitution efficiency of primitive HSCs (Figure S3).

Peripheral blood cell counts were similar in mice injected with either WT or *Prtn3*$^{-/-}$ LSK cells (Figure 4B). However, in mice injected with *Prtn3*$^{-/-}$ donor LSK cells competing against WT donor LSK cells, we noted a dramatic increase in *Prtn3*$^{-/-}$ donor-derived chimerism in LSK and LK cells in the BM (Figure 4C). There was also a higher frequency of *Prtn3*$^{-/-}$ donor-derived myeloid and B cells in the BM (Figure 4D). Similar to BM cells, *Prtn3*$^{-/-}$ donor-derived chimerism outcompeted that of WT donor in different lineages in peripheral blood (Figure 4E). Control mice reconstituted with competing congenic WT (CD45.2) and WT (CD45.1) LSK cells did not show any difference between the two congenic groups (Figures 4C–4E). In this setup, reconstitution efficiency of WT and *Prtn3*$^{-/-}$ LSK cells was assessed in the same BM environment at 16 weeks post transplant. Thus, the higher reconstitution efficiency observed in *Prtn3*$^{-/-}$ LSK recipients suggests that the augmented hematopoiesis induced by *Prtn3* disruption is an intrinsic feature of *Prtn3*-deficient HSCs.

Prtn3 Deficiency in HSPCs Does Not Affect Proliferation but Decreases the Rate of Apoptosis

The enhanced stem and progenitor cell compartments in *Prtn3*$^{-/-}$ mice prompted us to investigate the underlying mechanism. We first explored HSPC proliferation using a bromodeoxyuridine (BrdU) incorporation assay and DNA staining with 7-aminoactinomycin D (7-AAD) to analyze the frequency of LSK cells at different stages of the cell cycle. The percentage of LSK cells at different cell cycle phases (S/G2/M) was similar in WT and *Prtn3*$^{-/-}$ mice at 24 or 72 hr post BrdU injection (Figures 5A–5C). Although *Prtn3*$^{-/-}$ mice had a higher number of BrdU^{+} cells in the BM, this may have been due to increased number of HSPCs. The proportions of BrdU^{+} cells in the LSK subpopulations were similar in the BM of WT and *Prtn3*$^{-/-}$ mice (Figure 5C). We also investigated the rate of cell proliferation by Ki67 staining to analyze the frequency of cells in G1 phase. Similarly, the frequencies of LSK cells and LSK subpopulations in G1 phase were also comparable between WT and *Prtn3*$^{-/-}$ mice (Figures 5D and 5E). These data exclude the possibility that proliferation is responsible for the enhanced stem cell population seen in *Prtn3*$^{-/-}$ mice.

We recently reported that PR3 regulates neutrophil spontaneous death by cleaving and activating pro-caspase-3 (Loison et al., 2014). We therefore wondered whether PR3 regulated HSPC numbers by modulating their survival. To test this possibility, we first assessed spontaneous HSPC death using annexin V/7-AAD staining with freshly isolated BM cells from WT and *Prtn3*$^{-/-}$ mice; the frequencies of viable, early apoptotic, and late apoptotic cells in the stem and progenitor cell-containing populations were comparable in both groups (Figure S4A).

Since macrophages clear apoptotic cells, we decided to deplete BM macrophages using clodronate liposomes as previously described (Giuliani et al., 2001) and then examine LSK cell viability. BM macrophages remain markedly depleted for up to 2 weeks following clodronate liposome injection (Chow et al., 2011). At 9 days after injection, clodronate liposomes depleted 80% of Gr1^{-}CD115^{-}F4/80^{+} SSC-A^{normal} BM macrophages in both WT and *Prtn3*$^{-/-}$ mice, with no difference in the proportion of BM macrophages observed between clodronate or PBS liposome-treated WT and *Prtn3*$^{-/-}$ mice (Figures 6A and 6B). On day 9 post clodronate liposome injection, the frequency of viable LSK cells (Annexin V^{-}7-AAD^{-}) was higher and the frequency of late apoptotic LSK cells (Annexin V^{+}7-AAD^{+}) was lower in *Prtn3*$^{-/-}$ BM compared with WT BM (Figure 6C). Of note, both WT and *Prtn3*$^{-/-}$ BM contained very few early apoptotic LSK cells (Annexin V^{+}7-AAD^{-}), suggesting that early apoptotic LSK cells might be quickly converted to Annexin V^{+}7-AAD^{+} cells in the BM.

PR3 regulates neutrophil spontaneous death by cleaving and activating pro-caspase-3 (Loison et al., 2014). We tested if this mechanism also explained the reduced spontaneous death of LSK cells in *Prtn3*$^{-/-}$ mice. Using a fluorescent probe, we stained for active caspase-3 in LSK cells following macrophage depletion in the BM. Indeed, *Prtn3*$^{-/-}$ LSK cells exhibited significantly less active caspase-3, suggesting that delayed spontaneous death may well be due to a defect in pro-caspase-3 cleavage by PR3 (Figure 6D). The rates of apoptosis and caspase-3 activation were similar between WT and *Prtn3*$^{-/-}$ mice when mice were treated with PBS liposomes, confirming that the difference was macrophage dependent (Figures S4B and S4C). Taken together, these results demonstrate that *Prtn3*$^{-/-}$ LSK cells exhibit a reduced rate of apoptosis compared with WT LSK cells, which is best observed after depletion of BM macrophages.

In another set of experiments, sorted LSK cells from WT or *Prtn3*$^{-/-}$ mice were cultured in a stem cell maintenance medium containing various recombinant cytokines as described previously (Janzen et al., 2008). Annexin V/7-AAD staining was performed at 36 hr post culture. We observed a higher frequency of viable cells in *Prtn3*$^{-/-}$ LSK cultures compared with WT LSK cultures (Figure 6E). In addition, we performed a luminescence-based caspase-3 activity assay after a short-term culture of sorted LSK cells (as described in Flach et al., 2014). This assay revealed a 40% and 50% reduction in caspase-3 activity in *Prtn3*$^{-/-}$ LSK cells at 12 hr and 36 hr post culture, respectively

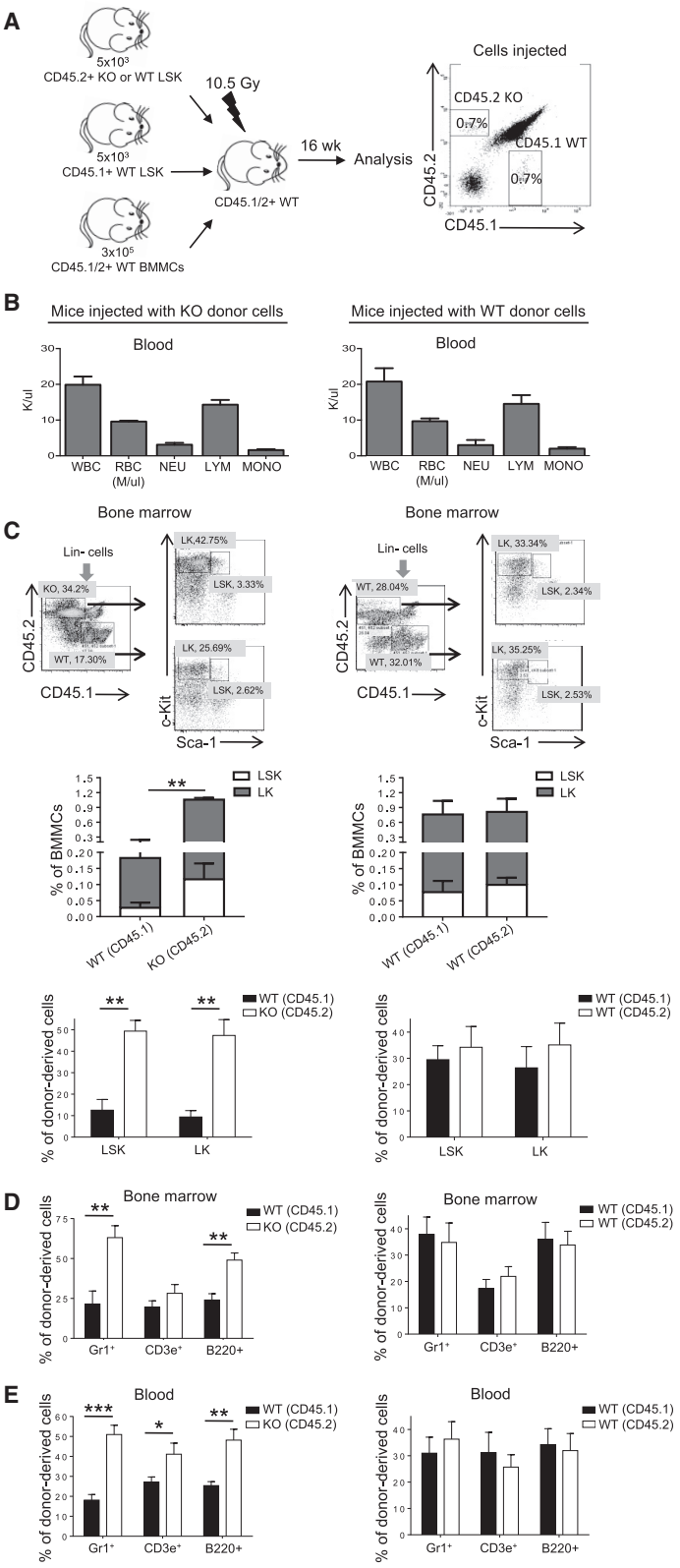

Figure 4. Elevated Hematopoiesis Caused by PR3 Deficiency Is an Intrinsic Feature of LSK Cells

(A) Scheme of the experimental setup used to compare WT and *Prtn3*$^{-/-}$ LSK cells by competitive transplantation.

(B) Peripheral blood cell counts (n = 4 per group).

(C) Representative FACS plots showing WT and *Prtn3*$^{-/-}$ donor-derived LSK and LK cells in recipient mice are shown in the top panels. Numbers denote the frequency of specific cell populations among the parent gate. The frequency of WT and *Prtn3*$^{-/-}$ donor-derived LSK and LK cells among total BM cells is shown in the middle panels. The percentage of LSK and LK cells from individual donors is shown in the bottom panels (n = 4 per group).

(D and E) Quantitative analysis of the origin of cells in recipient mice at 16 weeks post transplantation in (D) the BM and (E) peripheral blood (n = 4–7 per group).

All values shown are means ± SEM. *p < 0.05, **p < 0.01, ***p < 0.001, by unpaired, 2-tailed Student's t test. See also Figure S3.

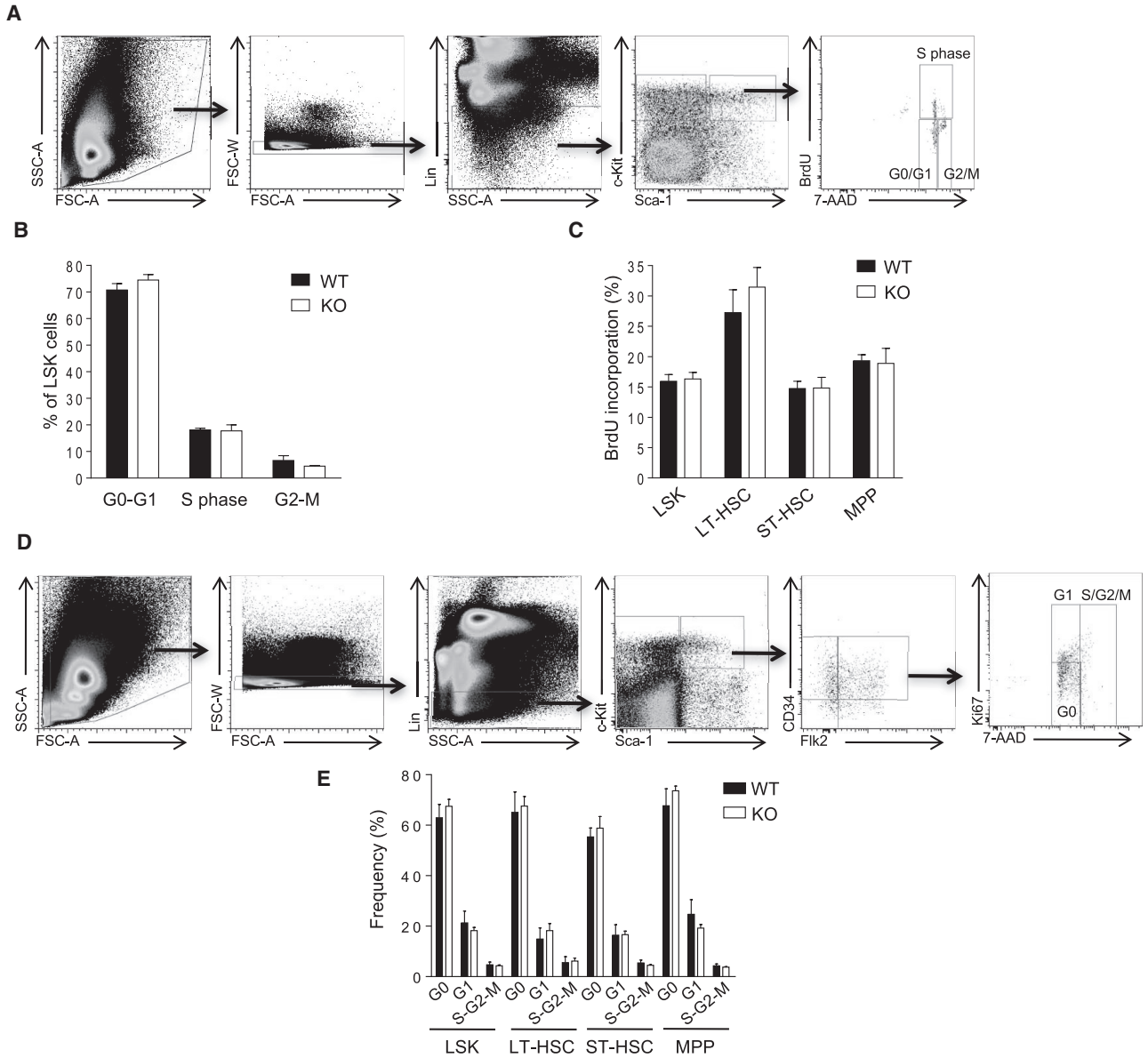

Figure 5. PR3 Does Not Affect Proliferation of Hematopoietic Stem and Progenitor Cells

(A) Gating strategy to analyze the cell cycle status of BM LSK cells by BrdU incorporation.

(B) Cell cycle analysis of LSK cells at 24 hr post BrdU injection (n = 4 per group).

(C) The rate of BrdU incorporation in LSK subsets at 72 hr post BrdU injection (n = 4 per group).

(D) Gating strategy to analyze the cell cycle status of BM LSK cells by Ki67 and 7-AAD staining.

(E) Cell cycle analysis of LSK subpopulations as assayed by Ki67 and 7-AAD staining (n = 4 per group).

See also Figure S4.

(Figure 6F). Collectively, these *ex vivo* data further demonstrate that *Prtn3*$^{-/-}$ LSK cells exhibit a reduced rate of apoptosis, at least partially due to reduced caspase-3 activation.

Next, we tested if HSPCs from *Prtn3*$^{-/-}$ mice are more resistant to irradiation. Although untreated *Prtn3*$^{-/-}$ LSK cells had a lower rate of apoptosis than WT counterparts, the rate of irradiation-induced apoptosis was similar between WT and *Prtn3*$^{-/-}$ LSK cells (Figure S5). In addition, we examined irradiation-induced apoptosis of LSK and LK cells *in vivo* (Shao et al., 2010; Yu et al., 2010). Similarly, we found that HSPCs from *Prtn3*$^{-/-}$ mice were not more

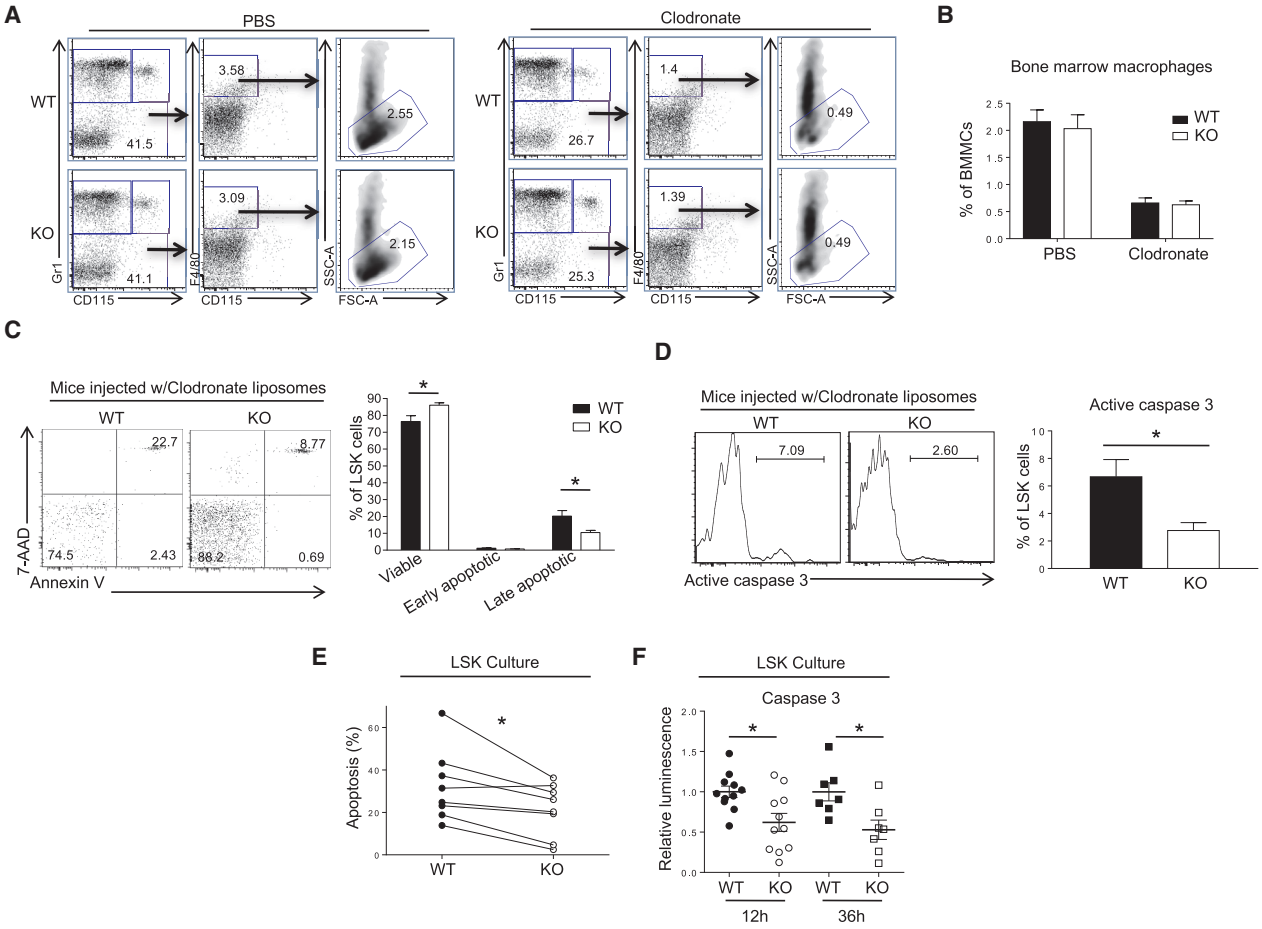

Figure 6. PR3 Regulates the Apoptosis of Hematopoietic Stem and Progenitor Cells

(A) Gating strategy to identify macrophage frequency in BM after treatment with PBS or clodronate liposomes. Numbers denote the frequency of specific cell subsets among live singlets.

(B) Quantification of BM macrophage frequency in WT and *Prtn3*$^{-/-}$ mice after liposome injection (n = 13–18 per group).

(C) Frequency of viable (Annexin V^{-} 7-AAD^{-}), early apoptotic (Annexin V^{+} 7-AAD^{-}), and late apoptotic (Annexin V^{+} 7-AAD^{+}) LSK cells in WT and *Prtn3*$^{-/-}$ mice after BM macrophage depletion. Numbers denote the frequency of cells among LSK cells (left panel). Quantification is shown in the right panel (n = 12–13 per group).

(D) Caspase-3 activation in LSK cells using a cell-permeable, fluorescent caspase-3 substrate. Numbers denote the frequency of LSK cells with active caspase-3 (left panel). Quantitative analysis is shown in the right panel (n = 5 per group).

(E) Apoptosis in sorted LSK cell cultures at 36 hr. Rate of apoptosis is calculated relative to the initial number of cells. %Apoptosis = (initial number of cells – total number of Annexin V^{-} 7-AAD^{-} cellular events detected)/initial number of cells (n = 8 per group).

(F) Analysis of caspase-3 activity in sorted LSK cells using a luminescence-based assay at 12 or 36 hr post culture. Data were normalized to the average luminescence value of WT cells for each independent experiment (n = 7–11 per group).

See also Figures S5 and S6.

resistant to irradiation (Figure S6). Collectively, these data suggest that the faster recovery observed in *Prtn3*$^{-/-}$ mice after sublethal irradiation and enhanced survival after lethal irradiation were likely due to an enlarged HSC pool size, instead of intrinsically increased resistance to irradiation. Thus, PR3 plays a critical role in the spontaneous death but not in irradiation-induced apoptosis of HSPCs. This is consistent with the current understanding that irradiation-induced apoptosis is mainly controlled by canonical caspase-mediated mechanisms.

DISCUSSION

Here, we reveal that *Prtn3*$^{-/-}$ BM has a higher number of HSPCs. Competitive reconstitution experiments suggest

that the expanded HSPC compartment is functional. Previous studies have shown that HSPCs with defective apoptosis display enhanced repopulation ability (Domen et al., 2000; Guo et al., 2010; Janzen et al., 2008). Since PR3 regulates spontaneous HSPC apoptosis by cleaving and activating pro-apoptotic caspase-3, our results identify PR3 as a regulator of HSPC number and function.

Prtn3 is a serine protease mainly expressed in granulocytes and a key player in innate immunity. Our findings suggest that PR3 is also an intrinsic regulator of the HSPC compartment in the BM. High *Prtn3* expression levels were detected in HSPCs. To our knowledge, *Prtn3* expression in HSPCs has not been reported. PR3 has been shown to play a role in neutrophil spontaneous death (Loison et al., 2014), and we now extend this finding to HSPCs, a population enriched with stem cells. While neutrophil spontaneous apoptosis is dependent on PR3-induced caspase-3 cleavage, caspase-8 and caspase-9 are not essential to this process but instead required for ligand-induced neutrophil apoptosis (Loison et al., 2014). Similarly, spontaneous apoptosis of HSPCs is likely also independent of caspase-8 or caspase-9, due to the absence of stimuli that trigger their activation under unchallenged hemostatic condition.

We previously demonstrated that pro-caspase-3 is a direct PR3 target (Loison et al., 2014). Similar to *Prtn3*$^{-/-}$ mice, caspase-3-deficient (*Caspase 3*$^{-/-}$) mice also have an expanded HSC pool (Janzen et al., 2008). Apoptosis was also decreased in *Caspase 3*$^{-/-}$ HSCs *in vitro* but, intriguingly, there was increased proliferation in *Caspase 3*$^{-/-}$ HSCs as a consequence of hyperactive cytokine signaling. Janzen et al. (2008) attributed the expanded HSC pool in *Caspase 3*$^{-/-}$ mice to increased proliferation rather than decreased cell death. However, we did not observe any differences in proliferation between WT and *Prtn3*$^{-/-}$ mice. Of note, non-apoptotic roles for caspase-3 in hematopoiesis such as regulation of lymphocyte proliferation (Woo et al., 2003), differentiation (Yi and Yuan, 2009), and the silencing of type I interferon production in dying cells to render mitochondrial apoptosis immunologically silent (White et al., 2014) have also been described. It remains to be determined whether PR3 contributes to these non-apoptotic caspase-3 functions in hematopoiesis. Importantly, we detected reduced apoptosis in *Prtn3*$^{-/-}$ LSK cells compared with WT LSK cells both *ex vivo* after short-term culture and *in vivo* after depletion of BM macrophages. We also examined the role of PR3 in irradiation-induced HSPC apoptosis. The rate of irradiation-induced apoptosis was similar between WT and *Prtn3*$^{-/-}$ LSK cells. In addition, HSPCs from *Prtn3*$^{-/-}$ mice were not more resistant to irradiation compared with HSPCs from WT mice. Collectively, our data indicate that PR3 plays a critical role in the spontaneous death, but not in irradiation-induced apoptosis, of HSPCs. This is consistent with the current understanding that irradiation-induced apoptosis is mainly controlled by canonical caspase-mediated mechanisms. It is likely that irradiation-induced HSPC apoptosis is dependent on caspase-8 and -9, while spontaneous HSPC apoptosis is mediated by PR3. The mechanism that leads to PR3 activation or *Prtn3* expression in HSPC needs to be further investigated.

Prtn3 expression in cultured CD34^{+} cells is regulated by granulocyte colony-stimulating factor and can confer cytokine-independent growth to BM-derived hematopoietic cells (Lutz et al., 2000). While this finding was obtained *in vitro* with progenitor cells, our *in vivo* data suggest that PR3 limits the HSPC compartment by driving the spontaneous turnover of HSPCs. In another study, PR3 inhibition arrested growth in a promyelocytic leukemia cell line, HL-60, and promoted granulocytic differentiation (Bories et al., 1989). Similarly, we observed preferential myeloid development in PR3-deficient BM, although a higher proportion of myeloid cells were immature. These discrepancies can be explained by the differential functions of PR3 in primitive HSCs and progenitor cells. Alternatively, the *in vitro* culture conditions may not closely resemble the *in vivo* BM environment for HSPC maintenance, self-renewal, and programmed death.

Intrinsic and extrinsic factors determine stem cell fate. HSPC pools undergo self-renewal and differentiation to ensure there are sufficient numbers of blood cells to fight infections and maintain homeostasis and host physiology. However, the number of HSPCs undergoing programmed cell death at a given point in time remains elusive. Various studies suggested a role for pro- and anti-apoptotic proteins in the quantitative and qualitative properties for HSPCs, confirming that cell death also plays a role in fate of HSPCs (Domen et al., 2000; Guo et al., 2010; Imai et al., 2010; Janzen et al., 2008; Opferman et al., 2005; V et al., 2010). Here, we identify PR3 as a regulator of HSPC survival and engraftment. PR3 inhibition might be useful to accelerate and increase the efficiency of myeloid reconstitution during BM transplantation especially when the number of donor cells is limited.

EXPERIMENTAL PROCEDURES

Mice

All experiments, unless otherwise noted, were performed on 8- to 12-week-old sex-matched mice. C57BL/6 WT and *Prtn3*$^{-/-}$ mice were bred in house in specific pathogen-free animal facilities at Boston Children's Hospital. *Prtn3*$^{-/-}$ mice were generated as previously described (Loison et al., 2014) and backcrossed to C57BL/6 mice for eight generations. B6.SJL-Ptprca Pepcb/BoyJ mice carrying CD45.1 allele were purchased from Jackson Laboratories and acclimated for 2 weeks. B6.SJL-Ptprca Pepcb/BoyJ mice and C57BL/6 mice were bred in house to generate mice carrying CD45.1 and

CD45.2 alleles. In all experiments with knockout mice, we used corresponding littermates as WT controls. All procedures were approved and monitored by the Children's Hospital Animal Care and Use Committee.

Complete Blood Count

Orbital peripheral blood (150 μL) was collected by heparinized capillary tubes (Fisher Scientific, 22-362-566) and transferred into K2-EDTA-coated tubes (Becton Dickinson, 365974). Blood parameters were analyzed by using Hemavet 950FS (Drew Scientific).

Flow Cytometry and Cell Sorting

BM cells from femurs and tibias were flushed into Dulbecco's PBS (Life Technologies, 14190-250) supplemented with 2% fetal bovine serum (FBS; Atlanta Biologicals, S11150H). Red blood cells were lysed by ACK buffer (Life Technologies, A10492-01). Five million BM cells were incubated with an antibody mixture including antibodies for lineage markers CD3e-APC (Biolegend, 100312), CD4-APC (Biolegend, 100516), CD8a-APC (Biolegend, 100712), CD11b-APC (Biolegend, 101212), CD45R/B220-APC (Biolegend, 103212), Gr1-APC (Biolegend, 108412), Ter119-APC (Biolegend, 116212), as well as Sca1-PE/Cy7 (Biolegend, 108114) and c-Kit-APC/Cy7 (Biolegend, 105826) in DMEM (Life Technologies, 31053-028) supplemented with 2% FBS. For LSK subset analysis, CD34-FITC (eBioscience, 11-0341-85) and CD135-PE (Biolegend, 135306) were used. Alternatively, CD48-PE (Biolegend, 103405) and CD150-PerCp/Cy5.5 (Biolegend, 115921) were used for LSK subsets. For LK subsets, CD34-FITC and CD16/32-PE (Biolegend, 101308) were used. Samples were incubated on ice for 15 min, then washed and filtered before analysis. When CD34 staining was performed, samples were stained for 1 hr on ice. For intracellular PR3 detection, BM cells were fixed and permeabilized using Intracellular Fixation & Permeabilization Buffer Set (eBioscience, 88-8824-00). The PR3 (D-20) antibody was purchased from Santa Cruz. For detection of apoptosis, cells were stained with antibodies against surface markers and then stained with annexin V-FITC (BD Biosciences, 556420) and 7-AAD (BD Biosciences, 559925) in annexin V binding buffer (BD Biosciences, 556454). To detect active caspase-3 by flow cytometry, a Vybrant FAM Caspase Assay Kit (Thermo Fisher Scientific, V35118) was used. Data were collected on FACSCanto II or LSR II flow cytometers (Becton Dickinson) and analyzed by FlowJo software (Tree Star).

For sorting highly purified cells, an immunomagnetic negative selection kit was used to enrich HSPCs (Stem Cell Technologies, 19756). Enriched cells were stained with Streptavidin-FITC (Biolegend, 405202), c-Kit-PE (Biolegend, 105808), and Sca1-APC (Biolegend, 108112). DAPI (BD Biosciences, 564907) was added to exclude dead cells. Cells were sorted on an Aria (Becton Dickinson) or MoFlo (Dako) cell sorter.

Bone Marrow Transplantation

Recipient mice carrying CD45.1 and CD45.2 alleles were γ-irradiated with two doses of 5.25 Gy. For total BM transplantation, recipients were injected with equal numbers of BM cells from each donor. For LSK transplantation, 5×10^3 sorted LSK cells from each donor (CD45.1 or CD45.2) were injected along with 3×10^5 supporting BM cells (CD45.1/2). Retroorbital bleeding was performed every 4 weeks. BM chimerism was analyzed at the end of each experiment. Gr1-FITC (Biolegend, 108406), CD45.1-PE (Biolegend, 110708), CD45.2-APC (Biolegend, 109814), CD3e-PE/Cy7 (Biolegend, 100320), and CD45R/B220-APC/Cy7 (Biolegend, 103224) were used to assess chimerism.

In Vivo Macrophage Depletion

Mice were injected with 250 μL of clodronate or PBS liposomes (ClodLip BV) intravenously at 9 days before tissue collection. BM macrophage depletion was confirmed using F4/80-FITC (Biolegend, 123108), Gr1-PE (Biolegend, 108408), and CD115-APC (Biolegend, 17-1152-82) antibodies.

Analysis of *In Vivo* Cell Proliferation by BrdU Incorporation

BrdU incorporation was assessed by a commercially available kit (BD Biosciences, 559619). Twenty-four to seventy-two hours before sacrifice, 2 μg of BrdU was injected intraperitoneally in 200 μL of PBS. At indicated time points, the frequencies of LSK, LT-HSC, ST-HSC, and MPP cells at different stages of the cell cycle were determined. In another set of experiments, Ki67-FITC (BD Biosciences, 556026) antibody was used to assess the frequency of cells in G1 phase.

Cell Culture

LSK cells (20,000–30,000) were directly sorted into 96-well round-bottom plates for annexin V/7-AAD staining, and 7,500–10,000 LSK cells in duplicates were sorted into solid white luminescence plates for detection of caspase 3-activity. LSK cells were cultured in Iscove's modified Dulbecco's medium (Life Technologies, 12440-053) supplemented with 5% FBS (Stem Cell Technologies, 06200), 100 U/mL penicillin, 100 μg/mL streptomycin (Life Technologies, 15140-122), 0.1 mM non-essential amino acids (Life Technologies, 11140-050), 1 mM sodium pyruvate (Life Technologies, 11360-070), 2 mM L-glutamine (Life Technologies, 25030-081), 50 μM β-mercaptoethanol (Life Technologies, 21985-023), recombinant murine stem cell factor (rmSCF; 25 ng/mL), recombinant murine thrombopoietin (rmTPO; 25 ng/mL), recombinant murine Flt-3 ligand (rmFlt-3L; 25 ng/mL), recombinant murine interleukin-3 (rmIL-3; 10 ng/mL), rmIL-11 (25 ng/mL), recombinant murine granulocyte macrophage colony-stimulating factor (rmGM-CSF; 10 ng/mL), and recombinant murine erythropoietin (rmEpo; 4 U/mL) for detection of caspase-3 activity as described previously (Flach et al., 2014). After 12–36 hr culture, caspase-3 activity was detected by using a luminescence-based Caspase-Glo 3/7 assay (Promega, G8090) according to the manufacturer's instructions. For annexin V/7-AAD staining, LSK cells were cultured in the presence of rmSCF (50 ng/mL), rmTPO (50 ng/mL), rmFlt-3L (50 ng/mL), and rmIL-3 (20 ng/mL) as previously described (Janzen et al., 2008). Annexin V/7-AAD staining was performed after 24–36 hr culture. In one set of experiments, cells were irradiated with 2 Gy right after purification. In another set of experiments, cells were cultured for 2 days and medium was replaced to contain rmFlt-3L (10 ng/mL) and rmIL-3 (10 ng/mL) for an additional 3 days as previously described (Janzen et al., 2008). On day 5, cells were

irradiated with 2 Gy. Annexin V/7-AAD staining was performed at 24 hr post irradiation. All recombinant cytokines were purchased from Peprotech.

PCR and Gene Expression Analysis

Prtn3 genotyping was done as described previously (Loison et al., 2014). RNA was isolated from fluorescence-activated cell sorted (FACS) BM subpopulations ($Gr1^+$ $CD11b^+$ neutrophils and $Lineage^-$ $Sca\text{-}1^+$ $c\text{-}Kit^+$ cells) using a Picopure RNA isolation kit (Thermo Fisher Scientific, KIT0204). cDNA was synthesized using an iScript cDNA synthesis kit (Bio-Rad, 1708891), and quantitative RT-PCR was performed using a SYBR Green Quantitative RT-PCR kit (Bio-Rad, 1708880). Primers used are listed below: *Prtn3*_fwd, 5′-CCCTGATC CACCCGAGATTC-3′; *Prtn3*_rev, 5′-GGTTCTCCTCGGGGTTGTAA-3′; *Gapdh*_fwd, 5′-AGAAGACTGTGGATGGCCCCTC-3′; *Gapdh*_rev, 5′-GATGACCTTGCCCACAGCCTT-3′.

Western Blot Analysis

Western blots were performed as previously described (Loison et al., 2014). Sorted LSK cells were loaded at a 1:1 ratio compared with LK cells and neutrophils. The antibodies against mouse PR3 (P-20) and gp91phox (54.1) were purchased from Santa Cruz. The antibody against mouse pan-actin (AAN01) was purchased from Cytoskeleton and GAPDH (MCA-1D4) was purchased from Encor.

Histological Analysis of Bone Marrow Smears

BM smears were prepared by squeezing the cells from femurs and tibias of mice directly onto slides. Cells were stained by a Diff-Quik Stain Kit (Siemens, B41312-1A) according to the manufacturer's instructions. At least 400 cells were counted to identify the lineage and maturation stage of BM cells. Investigators analyzing the samples were blinded to the identities of samples.

Colony-Forming Cell Assays

BM cells (2×10^4) and splenocytes (1×10^6) from WT and knockout mice were seeded in semisolid Methocult GF M3434 medium containing rmSCF, rmIL-3, recombinant human (rh)IL-6, and rhEpo for detection of colony-forming units-granulocyte, monocyte and burst-forming units-erythroid (Stem Cell Technologies, 03434). Colony numbers were counted on day 7, and images for colony sizes were obtained on day 8.

Statistical Analysis

All values shown are means ± SEM. Statistical significance for indicated datasets was performed by Student's t test on Prism (GraphPad). Unless otherwise indicated, data were analyzed using unpaired Student's t test. Viability and caspase-3 activity in sorted LSK cells as well as myeloid-lymphoid ratios in transplantation experiments were analyzed using paired Student's t test.

SUPPLEMENTAL INFORMATION

Supplemental Information includes six figures and can be found with this article online at https://doi.org/10.1016/j.stemcr.2018.10.004.

AUTHOR CONTRIBUTIONS

K.K., H.Z., J.M., Y.X., and H.R.L. conceived of the project. K.K., H.Z., X.Z., R.G., H.K., F.L., P.L., Q.R., H.Y., and X.L. designed/performed experiments and analyzed data. K.K. and H.R.L. wrote the manuscript. All authors contributed to the review of the manuscript. H.R.L., Y.X., F.M., and T.C. supervised the project. H.R.L. and Y.X. acquired the funds.

ACKNOWLEDGMENTS

The authors thank Joseph Mizgerd, Leslie Silberstein, and Li Chai for helpful discussions. We thank Li Zhao and Giri Buruzula for experimental support. This work was supported by the Non-profit Central Research Institute Fund of Chinese Academy of Medical Sciences (2018RC31002, 2017PT31033); the Chinese Academy of Medical Sciences (CAMS) Innovation Fund for Medical Sciences (2017-I2M-1-015); State Key Laboratory of Experimental Hematology Research Grant (157-Z18-01). Y.X. is supported by grants from National Basic Research Program of China (2015CB964903 and 2012CB966403), National Natural Science Foundation of China (31271484 and 31471116), and Natural Science Foundation of Tianjin City (12JCZDJC24600). H.R.L. is supported by NIH grants (R01AI103142, R01HL092020, and P01 HL095489) and a grant from FAMRI (CIA 123008). Cell sorting was performed at the HSCI/DRC Flow Core (NIH P30DK036836).

Received: November 27, 2017
Revised: October 2, 2018
Accepted: October 3, 2018
Published: November 1, 2018

REFERENCES

Bories, D., Raynal, M.C., Solomon, D.H., Darzynkiewicz, Z., and Cayre, Y.E. (1989). Down-regulation of a serine protease, myeloblastin, causes growth arrest and differentiation of promyelocytic leukemia cells. Cell *59*, 959–968.

Campanelli, D., Detmers, P.A., Nathan, C.F., and Gabay, J.E. (1990). Azurocidin and a homologous serine protease from neutrophils. differential antimicrobial and proteolytic properties. J. Clin. Invest. *85*, 904–915.

Chambers, S.M., Boles, N.C., Lin, K.Y., Tierney, M.P., Bowman, T.V., Bradfute, S.B., Chen, A.J., Merchant, A.A., Sirin, O., Weksberg, D.C., et al. (2007). Hematopoietic fingerprints: an expression database of stem cells and their progeny. Cell Stem Cell *1*, 578–591.

Cheshier, S.H., Morrison, S.J., Liao, X., and Weissman, I.L. (1999). In vivo proliferation and cell cycle kinetics of long-term self-renewing hematopoietic stem cells. Proc. Natl. Acad. Sci. U S A *96*, 3120–3125.

Chow, A., Lucas, D., Hidalgo, A., Mendez-Ferrer, S., Hashimoto, D., Scheiermann, C., Battista, M., Leboeuf, M., Prophete, C., van Rooijen, N., et al. (2011). Bone marrow CD169+ macrophages promote the retention of hematopoietic stem and progenitor cells in the mesenchymal stem cell niche. J. Exp. Med. *208*, 261–271.

Coeshott, C., Ohnemus, C., Pilyavskaya, A., Ross, S., Wieczorek, M., Kroona, H., Leimer, A.H., and Cheronis, J. (1999). Converting enzyme-independent release of tumor necrosis factor alpha and

IL-1beta from a stimulated human monocytic cell line in the presence of activated neutrophils or purified proteinase 3. Proc. Natl. Acad. Sci. U S A *96*, 6261–6266.

Domen, J., Cheshier, S.H., and Weissman, I.L. (2000). The role of apoptosis in the regulation of hematopoietic stem cells: overexpression of Bcl-2 increases both their number and repopulation potential. J. Exp. Med. *191*, 253–264.

Flach, J., Bakker, S.T., Mohrin, M., Conroy, P.C., Pietras, E.M., Reynaud, D., Alvarez, S., Diolaiti, M.E., Ugarte, F., Forsberg, E.C., et al. (2014). Replication stress is a potent driver of functional decline in ageing haematopoietic stem cells. Nature *512*, 198–202.

Florian, M.C., Dorr, K., Niebel, A., Daria, D., Schrezenmeier, H., Rojewski, M., Filippi, M.D., Hasenberg, A., Gunzer, M., Scharffetter-Kochanek, K., et al. (2012). Cdc42 activity regulates hematopoietic stem cell aging and rejuvenation. Cell Stem Cell *10*, 520–530.

Giuliani, A.L., Wiener, E., Lee, M.J., Brown, I.N., Berti, G., and Wickramasinghe, S.N. (2001). Changes in murine bone marrow macrophages and erythroid burst-forming cells following the intravenous injection of liposome-encapsulated dichloromethylene diphosphonate (Cl2MDP). Eur. J. Haematol. *66*, 221–229.

Guo, S., Lu, J., Schlanger, R., Zhang, H., Wang, J.Y., Fox, M.C., Purton, L.E., Fleming, H.H., Cobb, B., Merkenschlager, M., et al. (2010). MicroRNA miR-125a controls hematopoietic stem cell number. Proc. Natl. Acad. Sci. U S A *107*, 14229–14234.

Hyatt, G., Melamed, R., Park, R., Seguritan, R., Laplace, C., Poirot, L., Zucchelli, S., Obst, R., Matos, M., Venanzi, E., et al. (2006). Gene expression microarrays: glimpses of the immunological genome. Nat. Immunol. *7*, 686–691.

Imai, Y., Adachi, Y., Shi, M., Shima, C., Yanai, S., Okigaki, M., Yamashima, T., Kaneko, K., and Ikehara, S. (2010). Caspase inhibitor ZVAD-fmk facilitates engraftment of donor hematopoietic stem cells in intra-bone marrow-bone marrow transplantation. Stem Cell Dev. *19*, 461–468.

Janzen, V., Fleming, H.E., Riedt, T., Karlsson, G., Riese, M.J., Lo Celso, C., Reynolds, G., Milne, C.D., Paige, C.J., Karlsson, S., et al. (2008). Hematopoietic stem cell responsiveness to exogenous signals is limited by caspase-3. Cell Stem Cell *2*, 584–594.

Loison, F., Zhu, H., Karatepe, K., Kasorn, A., Liu, P., Ye, K., Zhou, J., Cao, S., Gong, H., Jenne, D.E., et al. (2014). Proteinase 3-dependent caspase-3 cleavage modulates neutrophil death and inflammation. J. Clin. Invest. *124*, 4445–4458.

Lutz, P.G., Moog-Lutz, C., Coumau-Gatbois, E., Kobari, L., Di Gioia, Y., and Cayre, Y.E. (2000). Myeloblastin is a granulocyte colony-stimulating factor-responsive gene conferring factor-independent growth to hematopoietic cells. Proc. Natl. Acad. Sci. U S A *97*, 1601–1606.

Notta, F., Zandi, S., Takayama, N., Dobson, S., Gan, O.I., Wilson, G., Kaufmann, K.B., McLeod, J., Laurenti, E., Dunant, C.F., et al. (2016). Distinct routes of lineage development reshape the human blood hierarchy across ontogeny. Science *351*, aab2116.

Opferman, J.T., Iwasaki, H., Ong, C.C., Suh, H., Mizuno, S., Akashi, K., and Korsmeyer, S.J. (2005). Obligate role of anti-apoptotic MCL-1 in the survival of hematopoietic stem cells. Science *307*, 1101–1104.

Orkin, S.H., and Zon, L.I. (2008). Hematopoiesis: an evolving paradigm for stem cell biology. Cell *132*, 631–644.

Shao, L., Sun, Y., Zhang, Z., Feng, W., Gao, Y., Cai, Z., Wang, Z.Z., Look, A.T., and Wu, W.S. (2010). Deletion of proapoptotic Puma selectively protects hematopoietic stem and progenitor cells against high-dose radiation. Blood *115*, 4707–4714.

Sieburg, H.B., Rezner, B.D., and Muller-Sieburg, C.E. (2011). Predicting clonal self-renewal and extinction of hematopoietic stem cells. Proc. Natl. Acad. Sci. U S A *108*, 4370–4375.

Sun, J., Ramos, A., Chapman, B., Johnnidis, J.B., Le, L., Ho, Y.J., Klein, A., Hofmann, O., and Camargo, F.D. (2014). Clonal dynamics of native haematopoiesis. Nature *514*, 322–327.

Takizawa, H., Regoes, R.R., Boddupalli, C.S., Bonhoeffer, S., and Manz, M.G. (2011). Dynamic variation in cycling of hematopoietic stem cells in steady state and inflammation. J. Exp. Med. *208*, 273–284.

V, M.S., Kale, V.P., and Limaye, L.S. (2010). Expansion of cord blood CD34 cells in presence of zVADfmk and zLLYfmk improved their in vitro functionality and in vivo engraftment in NOD/SCID mouse. PLoS One *5*, e12221.

White, M.J., McArthur, K., Metcalf, D., Lane, R.M., Cambier, J.C., Herold, M.J., van Delft, M.F., Bedoui, S., Lessene, G., Ritchie, M.E., et al. (2014). Apoptotic caspases suppress mtDNA-induced STING-mediated type I IFN production. Cell *159*, 1549–1562.

Woo, M., Hakem, R., Furlonger, C., Hakem, A., Duncan, G.S., Sasaki, T., Bouchard, D., Lu, L., Wu, G.E., Paige, C.J., et al. (2003). Caspase-3 regulates cell cycle in B cells: a consequence of substrate specificity. Nat. Immunol. *4*, 1016–1022.

Yi, C.H., and Yuan, J. (2009). The Jekyll and Hyde functions of caspases. Dev. Cell *16*, 21–34.

Yu, H., Shen, H., Yuan, Y., XuFeng, R., Hu, X., Garrison, S.P., Zhang, L., Yu, J., Zambetti, G.P., and Cheng, T. (2010). Deletion of Puma protects hematopoietic stem cells and confers long-term survival in response to high-dose gamma-irradiation. Blood *115*, 3472–3480.

Stem Cell Reports, Volume *11*

Supplemental Information

Proteinase 3 Limits the Number of Hematopoietic Stem and Progenitor Cells in Murine Bone Marrow

Kutay Karatepe, Haiyan Zhu, Xiaoyu Zhang, Rongxia Guo, Hiroto Kambara, Fabien Loison, Peng Liu, Hongbo Yu, Qian Ren, Xiao Luo, John Manis, Tao Cheng, Fengxia Ma, Yuanfu Xu, and Hongbo R. Luo

Supplemental Figures and Associated Legends (Figures S1-S6)

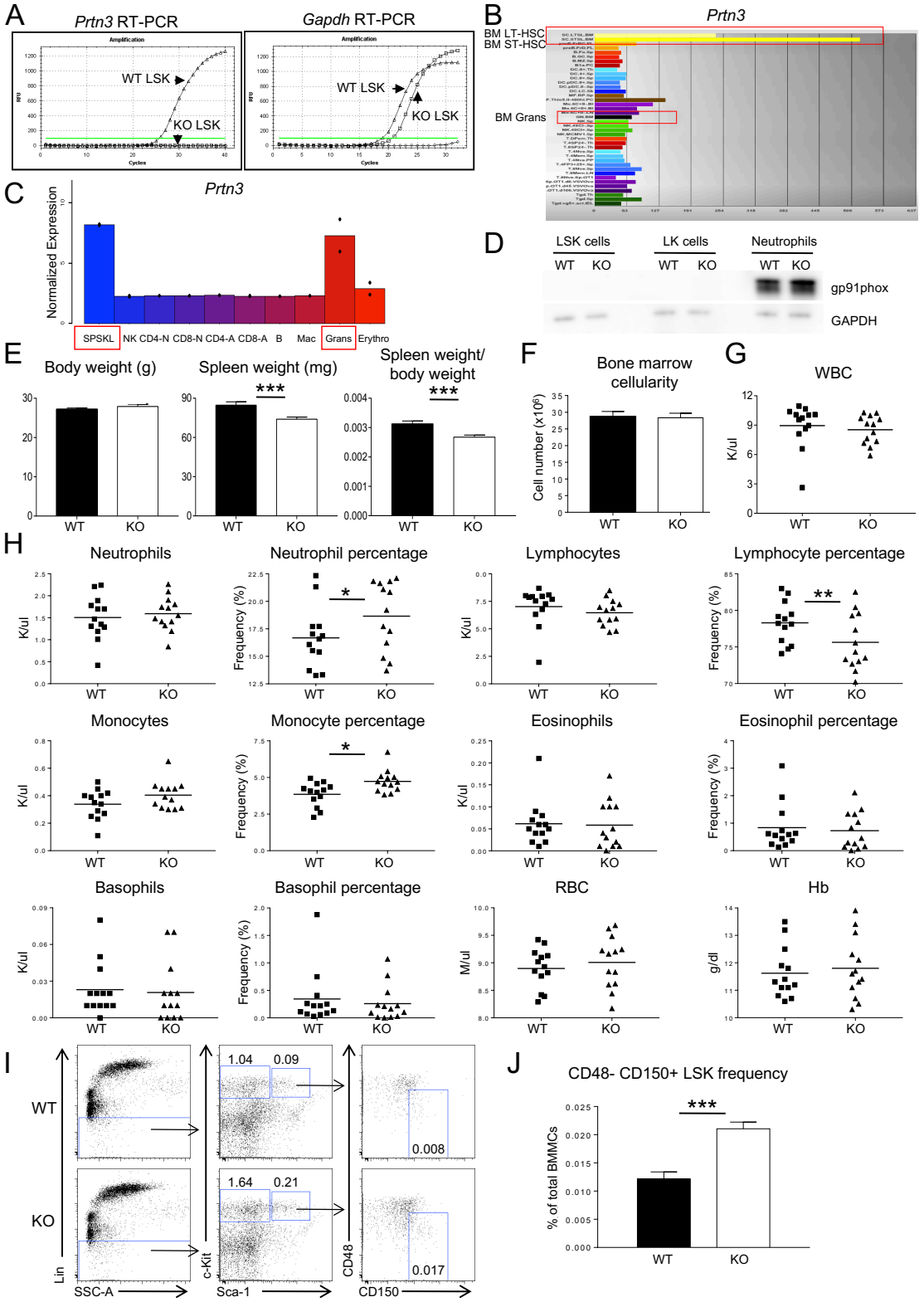

Figure S1. *Prtn3* expression in HSPCs and systemic parameters in *Prtn3*$^{-/-}$ mice. Related to Figure 1.

(A) Representative plots for *Prtn3* and *Gapdh* mRNA expression in sorted WT and *Prtn3*$^{-/-}$ LSK cells from three independent experiments.
(B) *Prtn3* mRNA expression in hematopoietic stem cells and neutrophils from the ImmGen Database. HSC and neutrophil populations are highlighted in red.
(C) *Prtn3* mRNA expression in hematopoietic stem cells and neutrophils from the Gene Expression Across Multiple Hematopoietic Lineages Database. HSC and neutrophil populations are highlighted in red.
(D) gp91phox was used to rule out neutrophil contamination in sorted LSK and LK cells and GAPDH was used as a loading control.
(E) Body weights, spleen weights, and spleen weight/body weight ratios of WT and *Prtn3*$^{-/-}$ mice (n=28).
(F) The number of BM mononuclear cells per one femur and one tibia in WT and *Prtn3*$^{-/-}$ mice (n=18).
(G) Total white blood cell counts in WT and *Prtn3*$^{-/-}$ mice (n=13).
(H) Numbers and percentages of different blood cell lineages and hemoglobin levels in WT and *Prtn3*$^{-/-}$ mice (n=13).
(I) Representative flow cytometry plots for CD48- CD150+ LSK cells in WT and *Prtn3*$^{-/-}$ mice. Numbers denote the frequency of each population among live singlets.
(J) Quantification of the frequency of CD48- CD150+ LSK cells in WT and *Prtn3*$^{-/-}$ mice (n=17). All values shown are mean ± SEM. *$p < 0.05$, ***$p < 0.001$, by unpaired, 2-tailed Student's t test.

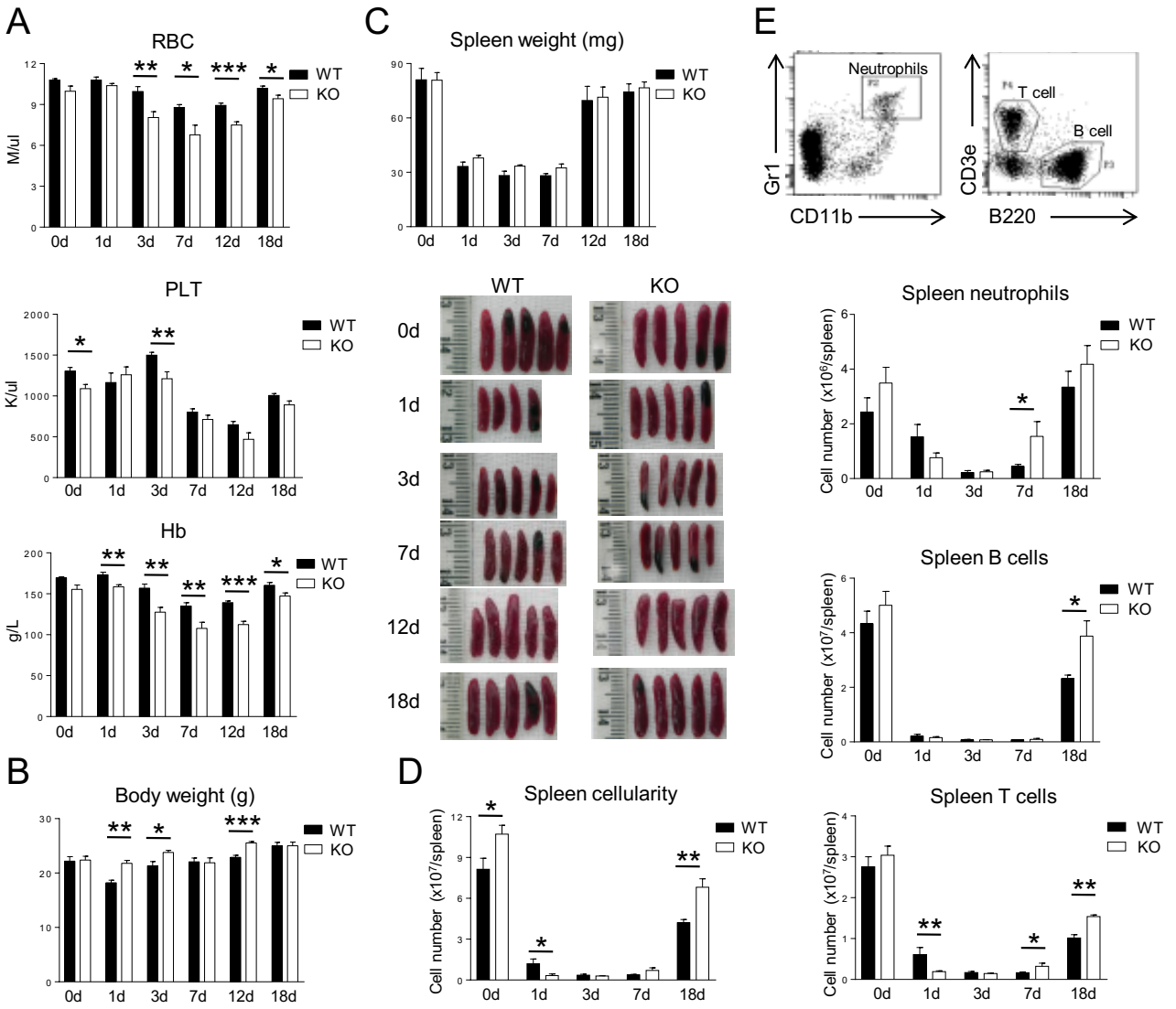

Figure S2. Additional information on the hematopoietic recovery of mice after sublethal irradiation. Related to Figure 3.
(A) Red blood cell, hemoglobin, and platelet counts in the peripheral blood of WT and *Prtn3*$^{-/-}$ mice before and after sublethal irradiation (n=5-9).
(B-C) Body weights and spleen weights of WT and *Prtn3*$^{-/-}$ mice before and after sublethal irradiation (n=5-9).
(D-E) Quantitative analysis of total mononuclear cells, neutrophils, B cells, and T cells in the spleen before and after sublethal irradiation (n=5-9). All values shown are mean ± SEM. *p < 0.05, **p < 0.01, ***p < 0.001, by unpaired, 2-tailed Student's t test.

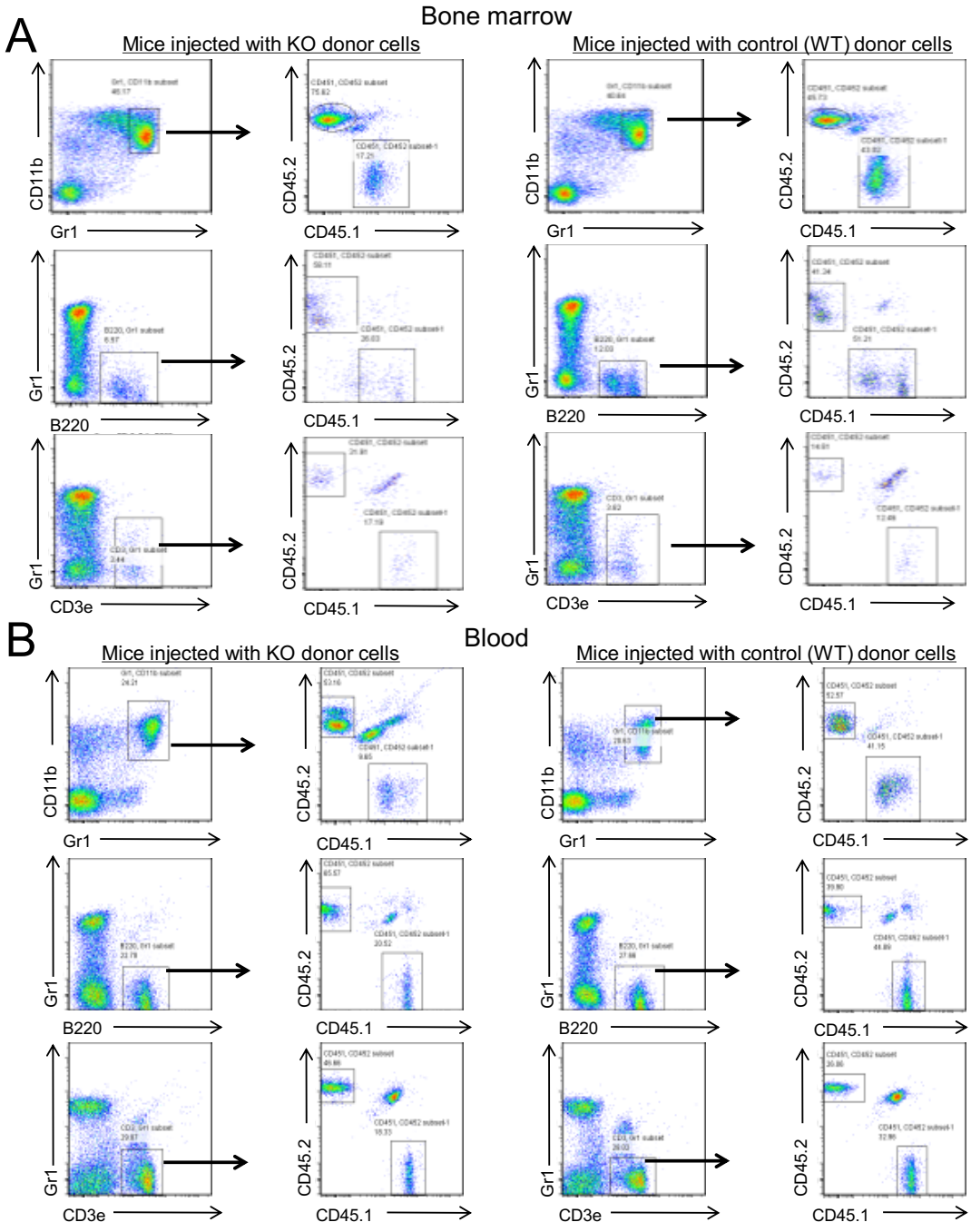

Figure S3. Gating strategy used in the transplantation study. Related to Figure 4.
(A) Gating strategy to analyze the chimerism of different donors of myeloid cells, B cells, and T cells in the BM of recipient mice.
(B) Gating strategy to analyze the chimerism of different donors of myeloid cells, B cells, and T cells in the peripheral blood of recipient mice.

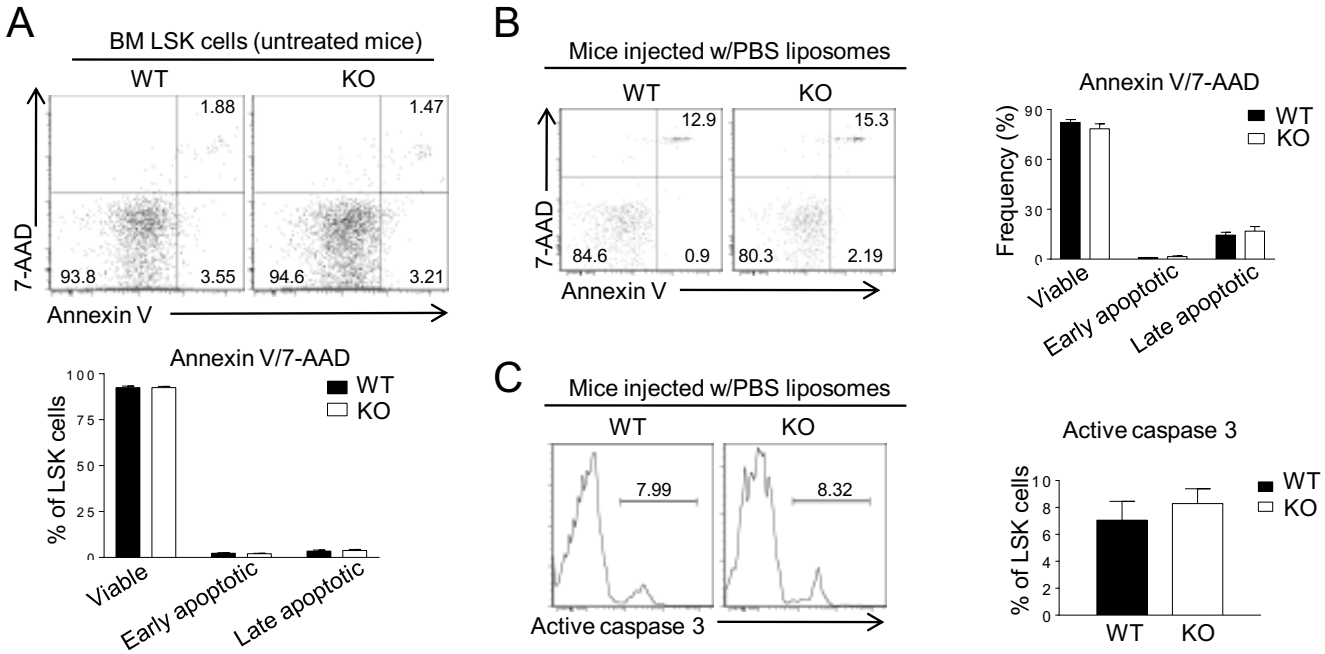

Figure S4. Additional information on the apoptosis of LSK cells from WT and *Prtn3*$^{-/-}$ mice. Related to Figure 5.
(A) Analysis of the frequency of viable (Annexin V^{-} 7-AAD^{-}), early apoptotic (Annexin V^{+} 7-AAD^{-}), and late apoptotic (Annexin V^{+} 7-AAD^{+}) LSK cells in untreated WT and *Prtn3*$^{-/-}$ mice (n=12-15).
(B) Analysis of the frequency of viable (Annexin V^{-} 7-AAD^{-}), early apoptotic (Annexin V^{+} 7-AAD^{-}), and late apoptotic (Annexin V^{+} 7-AAD^{+}) BM LSK cells in WT and *Prtn3*$^{-/-}$ mice after injection of PBS liposomes. Numbers denote the frequency of cells among LSK cells (left panel). Quantification of LSK viability is shown in the right panel (n=5).
(C) Representative FACS plots showing the frequency of BM LSK cells with active caspase 3 after treatment with PBS liposomes (left panel). Quantitative analysis of the frequency of LSK cells with active caspase 3 is shown in the right panel (n=5). All values shown are mean ± SEM. Statistical analysis was performed by unpaired, 2-tailed Student's t test.

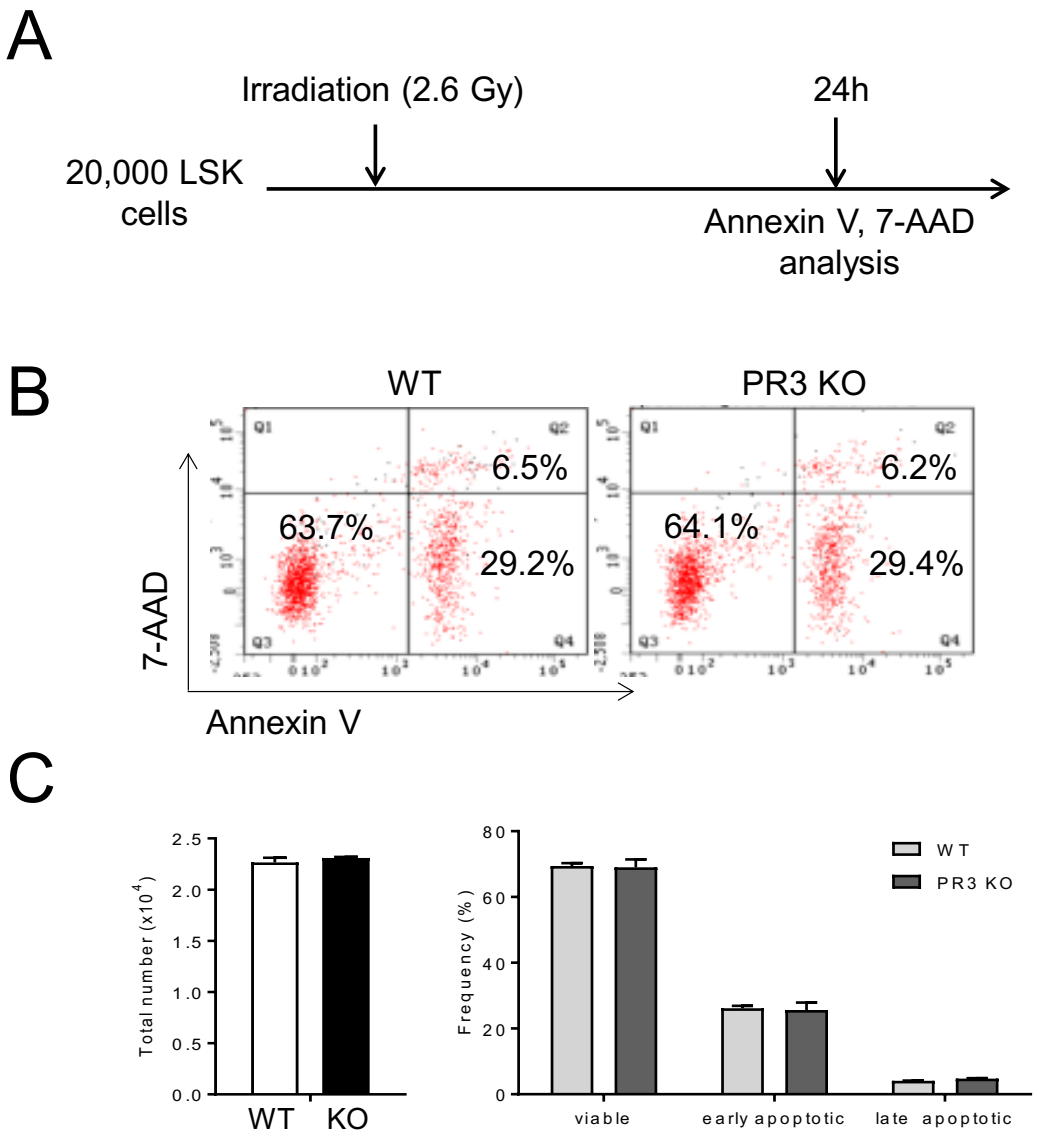

Figure S5. Irradiated WT and *Prtn3*$^{-/-}$ LSK cells displayed similar rate of apoptosis. Related to Figure 6.
(A) Scheme of the experimental setup.
(B) Gating strategy to identify viable (AnnexinV^{-}7/AAD^{-}), early apoptotic (AnnexinV^{+}/7-AAD^{-}), and late apoptotic (AnnexinV^{+}/7-AAD^{+}) cells.
(C) Number of viable cells was measured using Annexin V^{-} 7-AAD^{-} cellular events (n=4). Total cell numbers and the percentages of viable, early apoptotic, and late apoptotic cells in cultured WT and *Prtn3*$^{-/-}$ LSK populations were measured 24 hr after the irradiation. All values shown are mean ± SEM (n=4). This experiment was repeated twice and shown is a representative result of the two experiments performed.

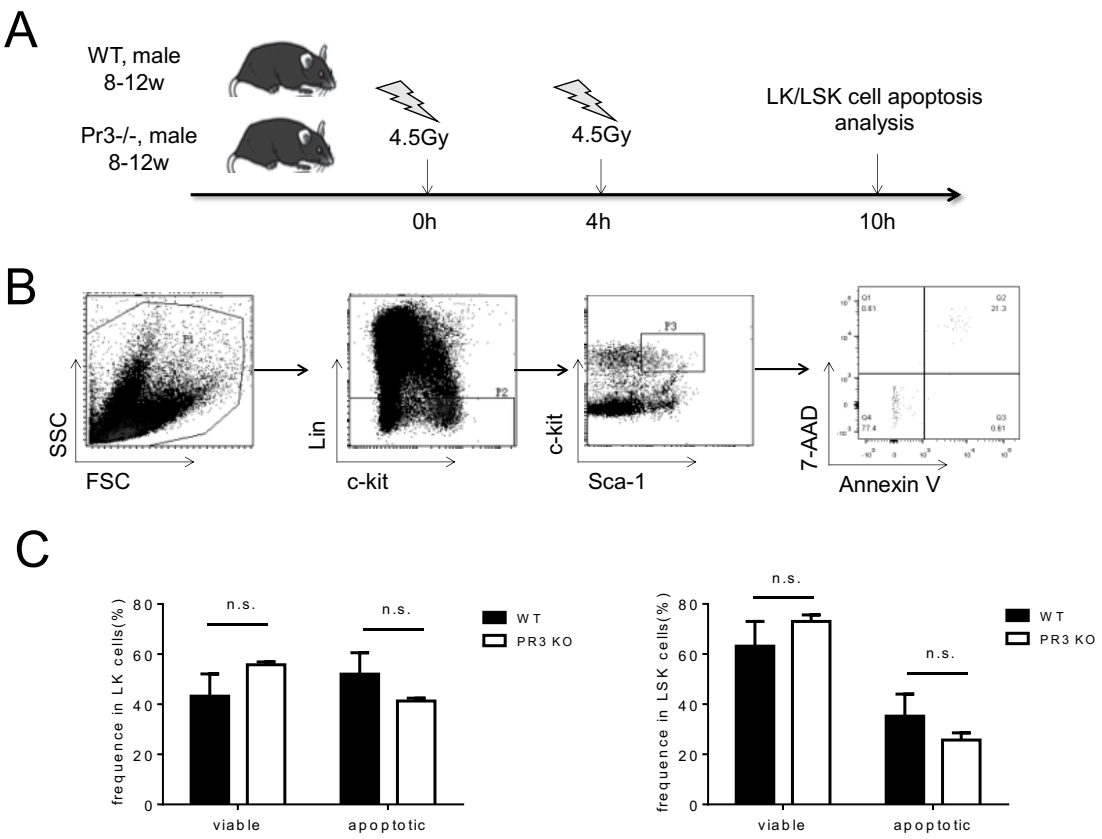

Figure S6. WT and *Prtn3*$^{-/-}$ HSPCs displayed similar rate of apoptosis in irradiated mice. Related to Figure 6.
(A) The experimental setup used to analyze HSPC apoptosis after challenge with sublethal irradiation. The dose of irradiation was chosen based on previous studies (Shao et al., 2010; Yu et al., 2010).
(B) Gating strategy to identify viable (AnnexinV^{-}7/AAD^{-}) and apoptotic (AnnexinV^{+} or 7-AAD^{+}) cells. (C) The percentages of viable and apoptotic cells in LK and LSK cell populations. All values shown are mean ± SD (n=3). n.s., not statistically significant ($P<0.05$) based on Student's t test.